

# Chemical double-mutant cycles: dissecting non-covalent interactions

Scott L. Cockroft and Christopher A. Hunter\*

Received 24th August 2006

First published as an Advance Article on the web 27th November 2006

DOI: 10.1039/b603842p

Thermodynamic double-mutant cycles and triple-mutant boxes are widely employed for the experimental quantification of non-covalent interactions and cooperative effects in proteins. This review describes the application of these powerful methodologies to the study of non-covalent interactions in synthetic systems.

## Introduction

In 1984, Fersht proposed a general thermodynamic cycle for the assessment of cooperative interactions on the substrate binding properties of an enzyme (Fig. 1).<sup>1</sup> If the change in free energy upon making a single X-mutation (e.g.  $\Delta G_{XY \rightarrow X'Y}$ ) differs from the free energy change when the same mutation is made to a single Y-mutant protein (e.g.  $\Delta G_{XY' \rightarrow X'Y'}$ ), then there must be an interaction between the mutated residues X and Y. Thus, the free energy difference between any two parallel mutations (e.g.  $\Delta G_{XY \rightarrow X'Y} - \Delta G_{XY' \rightarrow X'Y'}$ ) provides a measure of any direct or indirect interaction between residues X and Y:

$$\Delta\Delta G = \Delta G_{XY \rightarrow X'Y} - \Delta G_{XY' \rightarrow X'Y'} = \Delta G_{XY \rightarrow XY'} - \Delta G_{X'Y \rightarrow X'Y'} \quad (1)$$

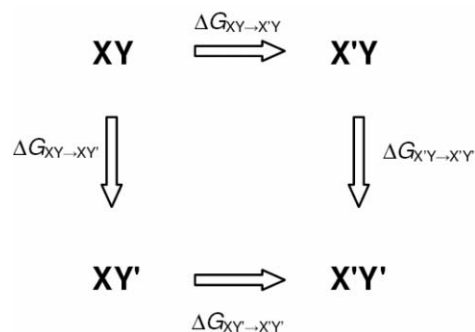
Fersht later described this thermodynamic relationship as a 'double-mutant cycle' (DMC)<sup>2</sup> and used this approach to quantify the interaction between charged residues in a barnase mutant.<sup>3</sup> In theory, a single mutant in which one or both of the charged residues were removed would be sufficient to assess the contribution of the interaction of interest. In practice, such

Centre for Chemical Biology, Department of Chemistry, Krebs Institute for Biomolecular Science, University of Sheffield, UK S3 7HF.  
E-mail: c.hunter@sheffield.ac.uk

an approach is often inappropriate because mutation of one residue disrupts multiple interactions with various parts of the protein. The DMC approach overcomes this problem, because the secondary free energy effects of the mutations cancel in a pairwise fashion in the thermodynamic cycle. Valid application of the DMC approach relies on certain criteria being met:

(i) Secondary perturbations must be additive functions of the mutations.

(ii) The mutant substitutions should be non-interacting, since the double mutant serves as the reference state.<sup>4,5</sup>



**Fig. 1** Schematic representation of the double-mutant cycle proposed by Fersht and co-workers for the assessment of side chain interactions using double-mutant proteins. Amino acid side chain X is mutated to X', and Y to Y'.



**Scott L. Cockroft**

doctoral position with Professor M. Reza Ghadiri at The Scripps Research Institute in California where he continues to pursue his

Scott Cockroft's interests in physical organic chemistry were sparked by an undergraduate placement at AstraZeneca R&D Charnwood, which formed part of his masters degree in chemistry (University of Manchester Institute of Science and Technology, 2002). He obtained his PhD (2006) under the supervision of Professor Chris Hunter at the University of Sheffield, where his research centred on the study of aromatic interactions.

Scott currently holds a post-



**Christopher A. Hunter**

various aspects of molecular recognition, design, synthesis, measurement and theory.

interests in molecular recognition phenomena.

Chris Hunter was educated at the University of Cambridge and graduated with a PhD in 1989. He was a lecturer at the University of Otago from 1989 till 1991, when he moved to the University of Sheffield. He was promoted to a personal chair in 1997, and he is currently an EPSRC Senior Research Fellow and Professor of Chemistry. He has research interests in

(iii) There should be no differences in the conformation of each member of the cycle. However, structural changes brought about by a single mutation do not necessarily preclude the use of this method. If similar structural transitions occur on both sides of the cycle, then the free energy differences will cancel in the analysis. Such pairwise conformational changes have been observed in structural studies of mutant proteins supporting the robust nature of the DMC approach.<sup>6</sup>

The use of DMCs for the quantification of non-covalent interactions in proteins is now standard practice.<sup>7,8</sup> This review deals with the use of DMCs in synthetic chemical systems. Although the methodology could also be used to quantify enthalpy and entropy changes, in the discussion that follows, we will focus exclusively on free energy changes. As we have pointed out previously, free energy tends to be a well-behaved thermodynamic parameter that provides insight into the contributions of functional group interactions, and it is much less sensitive to changes in structure and desolvation than enthalpy and entropy which tend to fluctuate in a mutually compensatory manner that can be tricky to disentangle.<sup>9</sup> When we refer to a functional group interaction or an interaction energy, these will always be free energies changes derived from experimental values of  $\Delta G^\circ = -RT \ln K$ .

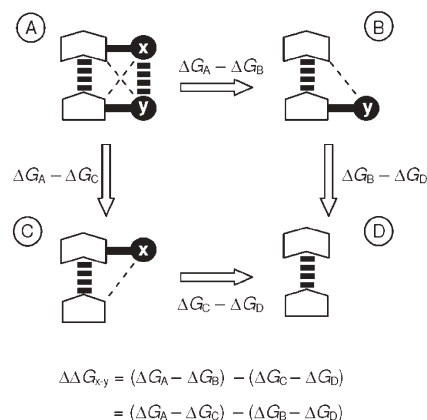
### Double-mutant cycles in synthetic chemical systems

Even the behaviour of the apparently simple synthetic systems can be perturbed by secondary effects that may not become apparent until the appropriate control experiments are performed. The DMC methodology, which has proved so valuable for the quantification of non-covalent interactions in proteins, can be used to dissect individual functional group interactions from the array of interactions typically present in a chemical system. The simplicity and limited degree of conformational freedom in synthetic systems means that secondary effects are likely to be additive.<sup>10–13</sup> Thus, the main requirements of the DMC approach can often be achieved without difficulty in well-defined chemical systems.

The approach is not suited to all situations. Obvious examples are provided by macrocycles and cavitands, where the molecular framework forms an essential part of a molecular recognition event. One mutant would require that the walls of the macrocycle were significantly altered, thereby destroying the complex of interest! DMCs have been used successfully in supramolecular complexes and folding molecules, and key examples will be discussed below.

### Interactions in supramolecular complexes

Fig. 2 shows a schematic representation of a DMC that can be used to quantify the intermolecular interaction between the x and y-groups in complex A. Each complex in the cycle must possess at least one intermolecular anchoring interaction, with the interaction of interest in another part of the complex that can be easily mutated. The x–y interaction is measured by chemical mutations which remove it. As before, a single mutation (*e.g.* comparing the stabilities of complexes A and B) is inadequate, because this has secondary effects such as changing the strength of the anchoring interaction or the interactions



**Fig. 2** General schematic representation of a supramolecular double-mutant cycle for measurement of the x–y interaction. The bold broken lines represent the major non-covalent interactions in the supramolecular complex, and the fine broken lines are the secondary effects that are cancelled in the cycle.

between the core of the complex and the x and y groups (thin dashed lines in Fig. 2). The double-mutant complex D quantifies these secondary effects and allows the contribution of the x–y interaction to the free energy of complexation to be quantified using the equation in Fig. 2. One of the main advantages of this approach is that both attractive and repulsive interactions can be quantified and that small thermodynamic contributions ( $\sim 1$  kJ mol<sup>-1</sup>) can be measured.

Aoyama used bifunctional metalloporphyrins that bind amino acids and amino esters to measure H-bonds in chloroform (Fig. 3).<sup>14</sup> The amino acid/ester mutant (2) was incapable of forming a H-bond with the phenolic group when bound to the metalloporphyrin (3). The mutant metalloporphyrin (4) does not possess a phenolic OH with the correct orientation to form a H-bond with the amino acid/ester anchored at the metal centre. Binding constants and hence free energies of complexation for each of the complexes A to D were obtained from spectrophotometric titrations. The thermodynamic analysis of these data was the equivalent of the DMC depicted in Fig. 3. For the methyl esters shown in Fig. 3, the H-bond was measured as  $-5.4$  kJ mol<sup>-1</sup>, and for the corresponding benzoic acids, the interaction was  $-11.3$  kJ mol<sup>-1</sup>.

Aoyama took advantage of the exceptionally well-defined bisnaphthol porphyrin framework in a second study (Fig. 4 and 5).<sup>15</sup> In these complexes, quinone derivatives (5, 6 and 9) are able to form H-bonds with the phenolic groups at the periphery of the porphyrin ring in addition to intermolecular face-to-face aromatic contacts. Using the published <sup>1</sup>H NMR titration data, the DMCs shown in Fig. 4 and 5 can be constructed. The complexation free energy differences have to be statistically corrected for complexes where degenerate binding modes are possible. In complexes C and D of Fig. 4, the free energy differences due these statistical effects cancel in the cycle. However, the four degenerate binding modes of complex B are not cancelled in the cycle, so this statistical correction is important. Using the DMC in Fig. 4, the second *intramolecular* anthraquinone (5) to phenol H-bond is determined to contribute  $-12.7$  kJ mol<sup>-1</sup> to the free energy of complexation with porphyrin 7 in CDCl<sub>3</sub> at 298 K. This

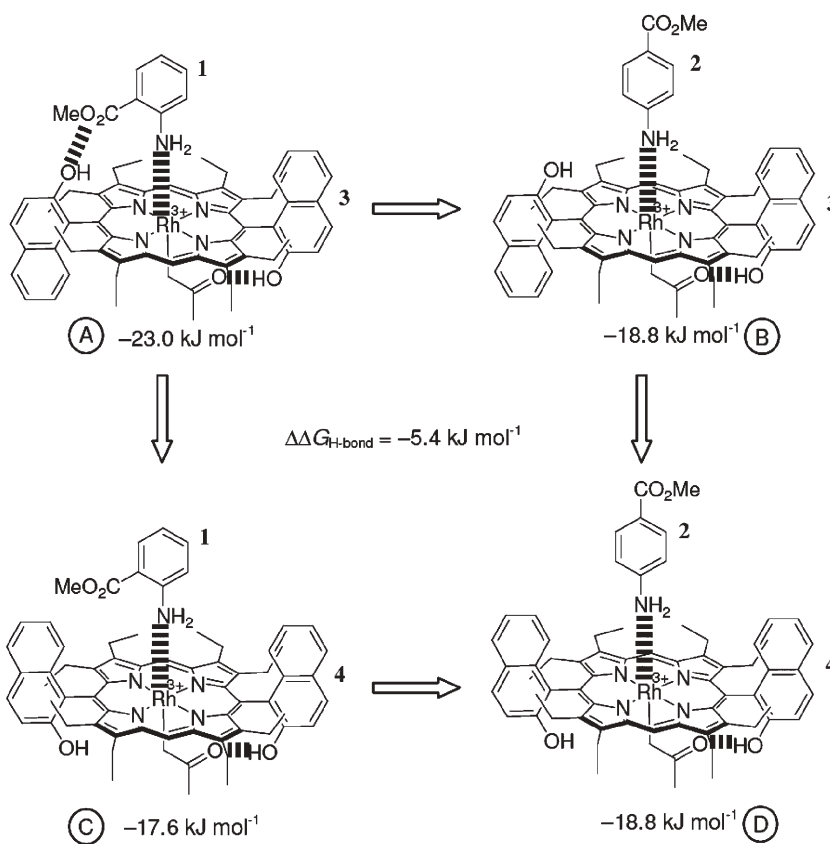


Fig. 3 Aoyama used bifunctional metalloporphyrins and this double-mutant cycle to elucidate the strength of the phenolic H-bond in complex A.

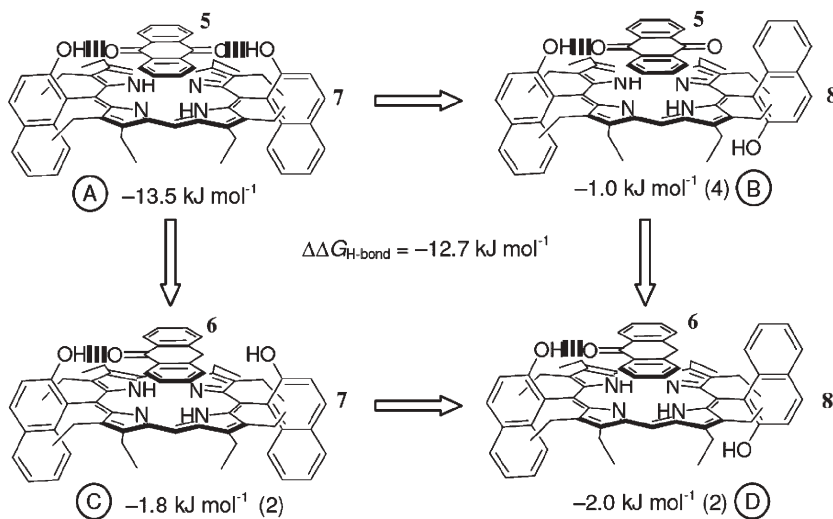
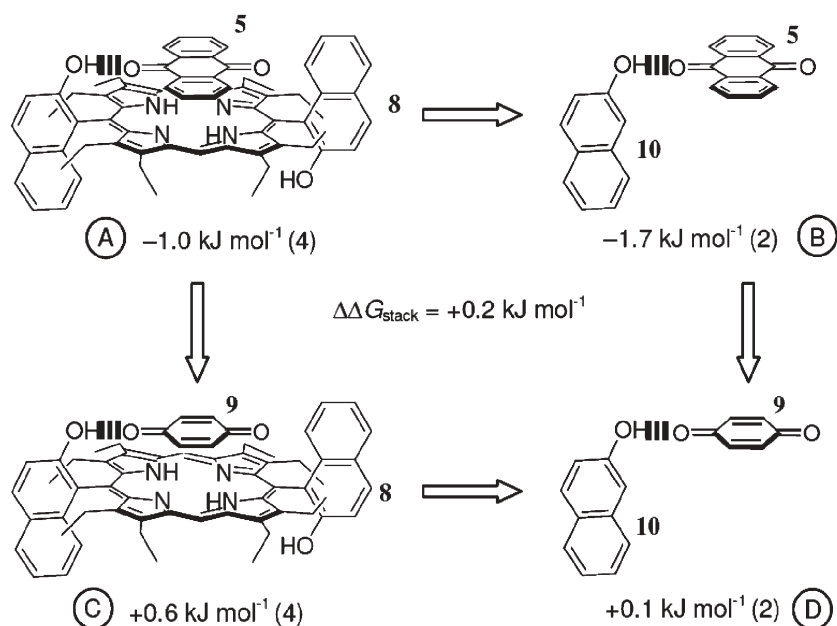


Fig. 4 Data obtained by Aoyama's studies of bifunctional porphyrins can be used with this double-mutant cycle to elucidate the strength of the intramolecular phenol-carbonyl H-bond in complex A in  $\text{CDCl}_3$  at 298 K. Statistical correction factors used for the complexation free energies are indicated in parentheses.

interaction energy appears to account for most of the total complexation free energy for the 5·7 complex ( $-13.5 \text{ kJ mol}^{-1}$ ). The reason is that formation of the first *intermolecular* H-bond must pay for the adverse free energy change associated with bimolecular association, which has been estimated to be  $6 \text{ kJ mol}^{-1}$ .<sup>9</sup> Using this approximation and assuming that each H-bond contributes  $-12.7 \text{ kJ mol}^{-1}$  to

the stability of the complex suggests that there are additional unfavourable interactions that destabilise complex A by about  $6 \text{ kJ mol}^{-1}$ . This difference could be due to repulsive aromatic stacking interactions in the 5·7 complex, which is consistent with the observation that benzoquinone (9), anthraquinone (5) and *p*-chloranil do not bind to a third porphyrin mutant bearing no hydroxyl groups in chloroform.



**Fig. 5** The data from Aoyama's studies can be used with this double-mutant cycle to investigate the stacking interaction between the outer aromatic rings of anthrone (**5**) and the porphyrin ring in  $\text{CDCl}_3$  at 298 K. Statistical correction factors used for the complexation free energies are indicated in parentheses.

Another DMC can be constructed to quantify this face-to-face aromatic contact, using the anthraquinone porphyrin complex, **5·8** (Fig. 5). In this DMC, benzoquinone (**9**) is used as one mutant, removing much of the extended aromatic surface of anthraquinone (**5**), and naphthol (**10**) is used as the other mutant, where the porphyrin ring is removed. For consistency, the free energies of complexation in Fig. 5 have been statistically corrected, although in this case, they cancel in the cycle. The DMC analysis shows that there is little interaction ( $+0.2 \text{ kJ mol}^{-1}$ ) between the outermost aromatic rings of anthraquinone (**5**) and the porphyrin (**8**). However, the A and C complexes in Fig. 5 are held together by only one H-bond, and so the aromatic rings are not forced to stack. In contrast to the anthraquinone porphyrin complex, **5·7**, where stacking is strictly enforced, the bound quinone in the **5·8** complex can move away from the porphyrin surface to minimise any repulsive stacking interactions.<sup>16</sup> The value of  $+0.2 \text{ kJ mol}^{-1}$  therefore represents a lower limit for the stacking interaction in the **5·7** complex. We can conclude that stacking interactions make an unfavourable free energy contribution to the stability of the **5·7** complex, but it is not possible to quantify the size of the repulsive interaction accurately. This highlights a general problem associated with measuring repulsive interactions. A highly constrained complex is required to force two groups that do not want to interact into an unfavourable geometry, because relatively small conformational changes are enough to completely remove the interaction. This example demonstrates how the individual free energy contributions of a complicated molecular recognition event can be dissected using DMCs.

Rebek used water-soluble receptors (**11** and **12**) for cyclic adenosine monophosphates (cAMP) to measure a phosphate-guanidinium interaction in water.<sup>17</sup> The synthetic receptors bind cAMP using a combination of hydrophobic, H-bonding

and electrostatic phosphate-guanidinium interactions (Fig. 6, complex A). In complexes C and D, the guanidinium group was mutated to a methyl group, and in complexes B and D, adenosine was used as the mutant guest, since it lacks the phosphate group of cAMP. Using DMCs similar to the one shown in Fig. 6, the strength of the phosphate-guanidinium interaction in complex A was estimated to be  $-2.5 \text{ kJ mol}^{-1}$  at 51 mM ionic strength and  $-1.2 \text{ kJ mol}^{-1}$  at 501 mM ionic strength. The authors noted that when 3',5'-cAMP is bound to **11**, two rotors are constrained relative to the complex with adenosine (**14**), so these values represent the lower limits of the interaction free energies.

### Edge-to-face aromatic interactions

We have used chemical DMCs for the quantification of a wide range of aromatic interactions in supramolecular complexes. These complexes are based on amide oligomers, molecular zippers, that form complexes in  $\text{CDCl}_3$  through a combination of H-bonds and edge-to-face aromatic interactions (Fig. 7).<sup>18,19</sup> Truncated zipper complexes that consist of one bisaniline derivative unit (e.g. **15** and **16**) and one isophthaloyl derivative (e.g. **17** and **18**) also form 1 : 1 complexes in  $\text{CDCl}_3$  solution (Fig. 8). Binding constants and therefore complexation free energies were determined using  $^1\text{H}$  NMR titrations. The geometries of the complexes have been confirmed using patterns in complexation-induced changes in chemical shift ( $\Delta\delta$  values) and ROESY experiments. The three-dimensional structures of zipper complexes in solution were determined from the  $\Delta\delta$  values and by comparison with the crystal structures of simple mono-amide model compounds.<sup>20–28</sup>

Zipper complexes are well-suited to the DMC approach, since the terminal amide groups can be readily mutated using simple synthetic procedures. Ideal mutant reference states

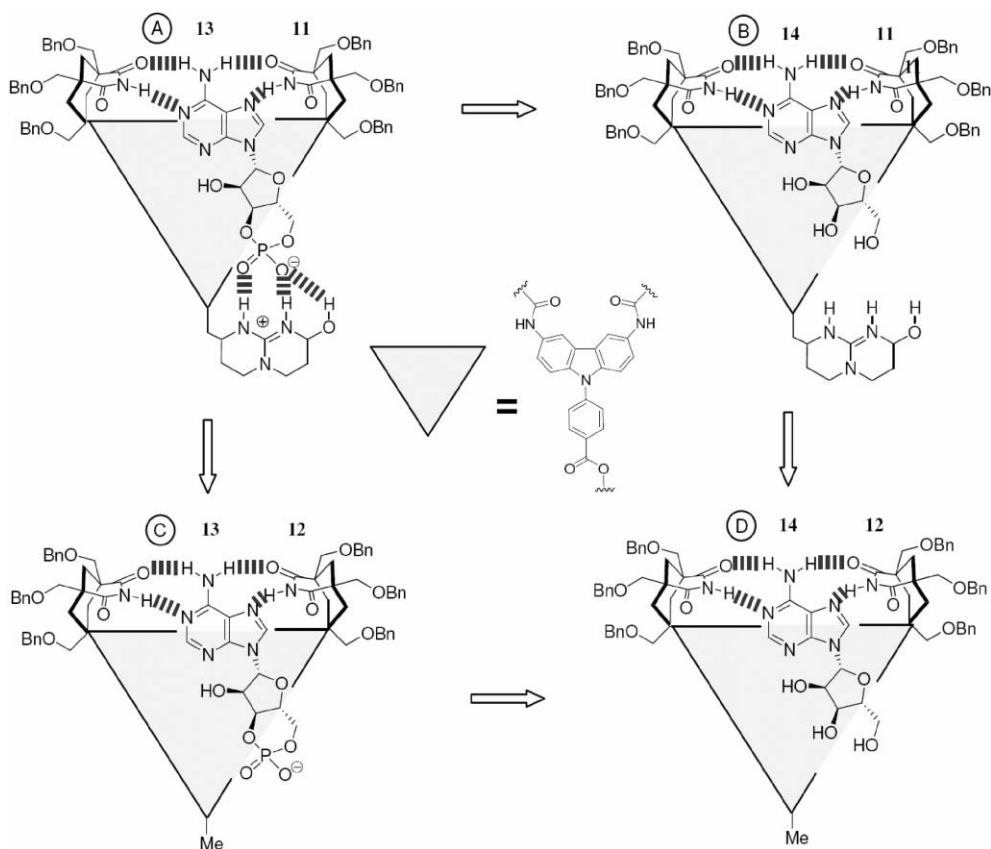


Fig. 6 Double-mutant cycle used by Rebek to quantify the phosphate–guanidinium interaction in H<sub>2</sub>O–D<sub>2</sub>O solution at 288 K, pH 6.

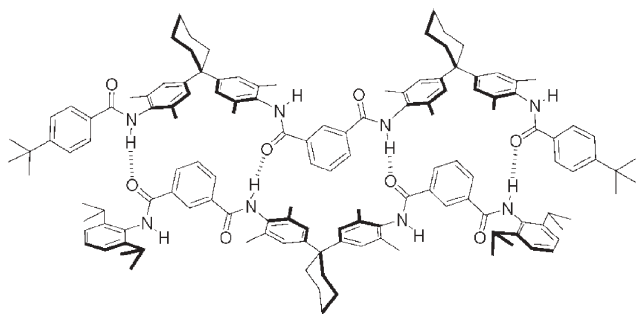


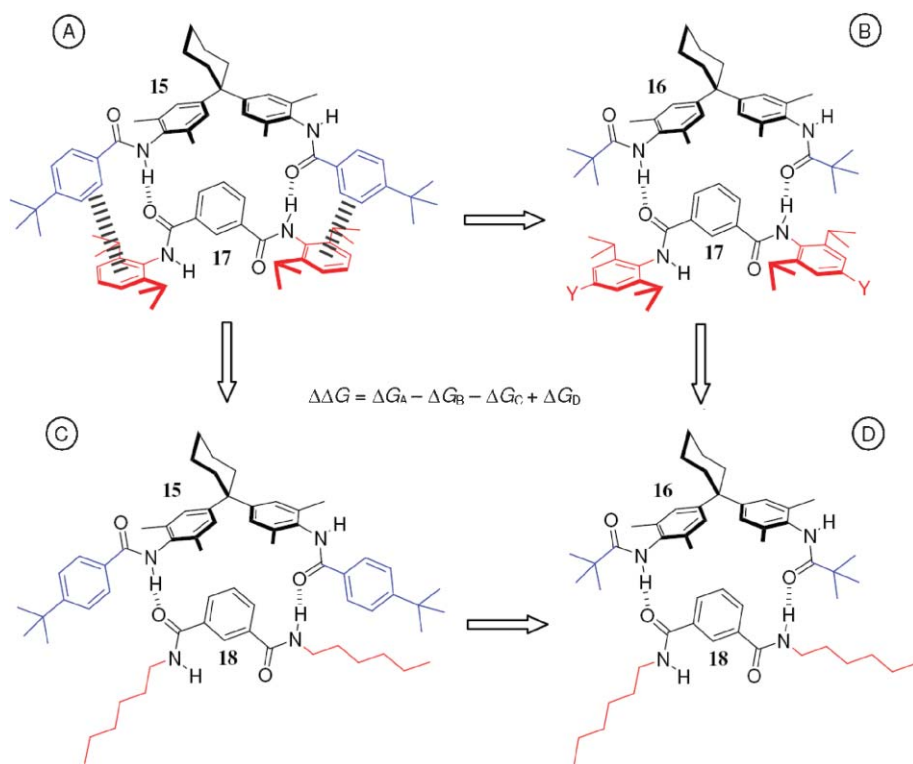
Fig. 7 A molecular zipper complex.

would completely remove the interacting groups of interest, thus exposing the other interacting partner to the solvent. In the case of the isophthaloyl derivatives (*e.g.* **17**), such mutants would be isophthalamide (hydrogen as the mutant group) or the *N*-methyl diamide (methyl as the mutant group), but these compounds have insufficient solubility in CDCl<sub>3</sub> for use in <sup>1</sup>H NMR titrations.<sup>29</sup> The next best solution is to use a mutant group that is weakly interacting. Therefore, the CDCl<sub>3</sub> soluble dihexyl isophthalimide (**18**) (*n*-hexyl as the mutant group) was used as the mutant control compound. For the bisaniline half of the complex, mutant groups with formyl amides (hydrogen as the mutant group) were abandoned due to the complexity of <sup>1</sup>H NMR spectra arising from *cis/trans* amide conformers.<sup>30</sup> Both methyl and *tert*-butyl have been used as mutant groups in bisaniline derivatives, and these appear to be interchangeable

with little effect on the binding constants.<sup>21</sup> The use of the alkyl mutant groups has an important implication for interpretation of the DMC results obtained in zipper complexes. Although binding constants are determined in CDCl<sub>3</sub>, the solvating CDCl<sub>3</sub> molecules are displaced from the functional groups of interest by the mutant alkyl groups, and the free energy effects of desolvation are (at least partially) cancelled in the DMC. This means that the interaction free energy differences in effect refer to an alkane–CDCl<sub>3</sub> pseudo-solvent mixture.

Another of the important assumptions of the DMC approach is that the secondary interactions and changes in H-bond strength are additive. The free energy contribution of a H-bond is proportional to the product of the H-bond acceptor and donor constants ( $\alpha$  and  $\beta$ ).<sup>9</sup> However, if the change in the H-bond polarities is small, then the change of the product is approximately equal to the change in the sum.<sup>21</sup> Since the  $\alpha$  and  $\beta$  values of amide groups bearing a range of electron-withdrawing and donating substituents vary by  $\pm 15\%$ , the additivity assumption should hold reasonably well. Experimental support for this hypothesis comes from the measured magnitudes of secondary interactions<sup>31</sup> and from triple mutant studies (see later).

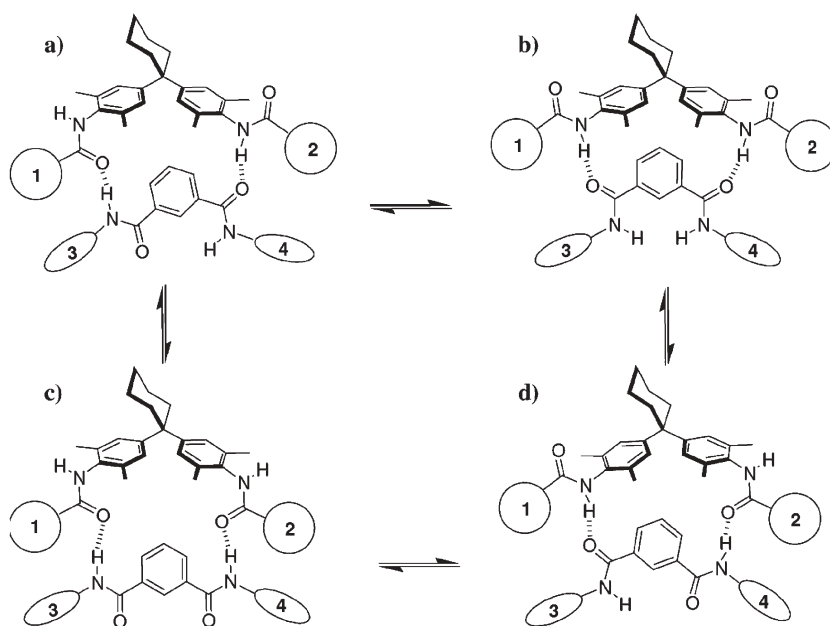
Fig. 8 shows one of our earliest DMCs. The similarity of these complexes to the original oligomeric molecular zippers is clear (*cf.* Fig. 7). There are multiple intermolecular anchoring interactions in these complexes: two amide–amide H-bonds, and two edge-to-face aromatic interactions with the



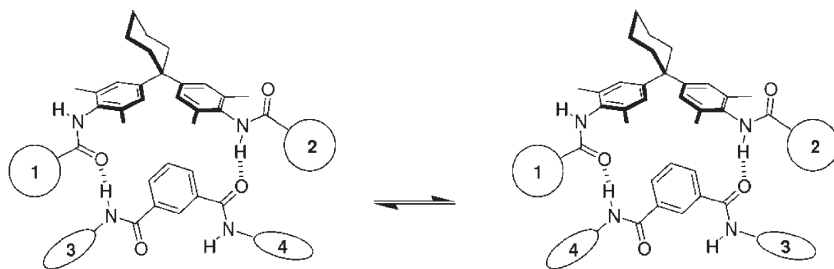
**Fig. 8** A double-mutant cycle for determining the magnitude of the two terminal edge-to-face aromatic interactions in complex A (15-17).

isophthaloyl group in the core of the complex. The geometry of complex A allows the magnitude of edge-to-face aromatic interactions to be determined using DMC methodology. Complex A contains two terminal edge-to-face aromatic contacts with subtly different geometries. Thus, the free energy determined in the DMC in Fig. 8 corresponds to the sum total of the two edge-to-face contacts. This analysis is actually an over-simplification, because each of the amide bonds in the

complex is able to act as a H-bond donor or acceptor. A full scheme of the conformational possibilities is shown in Fig. 9. DMCs performed using the zipper complexes actually measure the Boltzmann weighted average interaction energies of all accessible conformational states. The conformations shown in Fig. 9b and 9c are not expected to be highly populated because of the intramolecular electrostatic repulsion between the amides in the isophthaloyl derivatives, and this is supported



**Fig. 9** Conformational equilibria in molecular zipper complexes.



**Fig. 10** One example of the additional conformational equilibria that affect zipper complexes when both components are unsymmetrical (*i.e.* **1**  $\neq$  **2** and **3**  $\neq$  **4**).

by the experimentally determined NMR structures. The conformational equilibrium is simplified when both components of each complex in the DMC are symmetrical, because two of the conformational states are degenerate (Fig. 9a and 9d). Using the ‘symmetrical DMC’ shown in Fig. 8, the magnitude of one of the terminal edge-to-face aromatic interactions was determined to be  $-1.3 \text{ kJ mol}^{-1}$ .

The conformational situation is most complicated when both components of the zipper complex are unsymmetrical, because additional binding modes exist (Fig. 10). In these circumstances, conformational amide flipping has been shown to introduce a maximum error of  $0.8 \text{ kJ mol}^{-1}$ , which is similar to the error margin involved in the determination of the association constants.<sup>31</sup> Problematic conformational equilibria of the type shown in Fig. 10 are avoided by constructing DMCs where at least one component of each complex is symmetrical. Using this approach, two different ‘semi-symmetrical DMCs’ were constructed, and these gave values of  $-1.4$  and  $-1.6 \text{ kJ mol}^{-1}$  for the terminal edge-to-face aromatic interaction. These values are remarkably similar to the value obtained using the fully symmetrical DMC, which gives some indication of the robustness of the DMC analysis when applied to this system.<sup>21</sup> In a study conducted by Martínez, the design of the zipper complex was modified by replacing the central diphenylcyclohexyl group in the bisaniline derivative with a diphenylnorbornane group.<sup>32</sup> In this system, the edge-to-face interaction between two unsubstituted aromatic rings was measured as  $-0.2 \pm 0.6 \text{ kJ mol}^{-1}$  using the DMC approach, demonstrating the sensitivity of the interaction to changes in the geometry of the core of the complex.

Interaction energies determined using zipper complexes are not expected to be directly transferable to other systems but provide a useful indicator of the magnitude of the interactions involved. DMC studies conducted in our laboratory have focused on revealing the trends in interaction energies as the properties of the interacting groups are varied. These systematic studies provide a self-consistent overview of the effects of substituents on aromatic interactions, and the nature of non-covalent interactions in general. The results of these experimental DMC analyses are collected in Table 1, and the complexes used to obtain these values are discussed below.

Fully symmetrical DMCs were used to measure the interaction between the edge of a pyridine ring and the face of substituted aromatics using compound **19** (Fig. 11a).<sup>33</sup> The interaction was more favourable than the phenyl edge-to-face interaction, reflecting the increased partial positive charge of

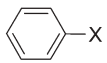

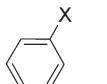

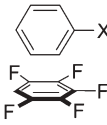

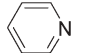

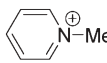

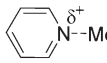

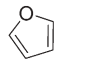



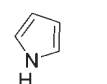


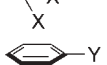
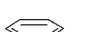
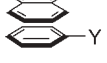


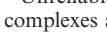
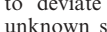
the edge of the pyridine ring compared with a benzene ring. When  $Y = \text{NMe}_2$ , the aromatic face is electron rich, and the interaction is most favourable, and when  $Y = \text{NO}_2$  the electron density at the aromatic face is depleted, and the interaction was the least favourable. It is important to point out that this trend in interaction energies as the Y-substituents are varied is a recurring pattern that affects all of the edge-to-face systems studied in zipper complexes (Fig. 12).

The interactions of the edge of five-membered heteroaromatics with the face of substituted aromatics were also investigated using symmetrical bisaniline derivatives **19–22** (Fig. 11a).<sup>33</sup> For these compounds the use of fully symmetrical DMCs were required because of the asymmetry of the five-membered rings: the heteroatoms are free to point towards, or away from, the aromatic face, making the conformational equilibrium in Fig. 9 even more complicated. Once again, the interaction free energies represent the Boltzmann weighted average of all of the possible conformational states. The interactions of furan (**20**) and thiophene (**21**) with the face of an aromatic group were similar. The pyrrole group (**22**) was found to interact very favourably with the face of aromatic rings, stabilising the complex by at least  $4.7 \text{ kJ mol}^{-1}$  when  $Y = \text{H}$ . Pyrrole interacts more favourably with the face of an aromatic ring than the edges of a phenyl, pyridine, furan or thiophene group, because the NH of the pyrrole has by far the largest partial positive charge.<sup>33</sup>

The pyrrole-interaction has also been investigated using the semi-symmetrical zipper complexes shown in Fig. 13a. Pyridine is a strong electron-withdrawing group, and this has two effects on the complexes used in the DMC. Firstly, it increases the binding constants of the complexes, because the polarity of the NH in the amide adjacent to the pyridine group is increased. This serves as a conformational lock and fixes the conformational equilibrium in the geometry shown in Fig. 13a, where the pyrrole NH is H-bonded to the aromatic face. Compound **25** was also found to bind the mutant isophthaloyl derivative **18** in an unexpected way (Fig. 13b). When the isophthaloyl binding partner does not contain an aromatic group, the pyrrole NH of **25** makes a second H-bond to one of the amide carbonyl oxygens of **18**. Due to this conformational change, the DMC could only be used to assign an upper limit for the interaction free energy as  $-4.5 \text{ kJ mol}^{-1}$ , which is consistent with the slightly more favourable interaction found in the fully symmetrical complex shown in Fig. 11a.<sup>34</sup>

An even clearer view of the effects of substituents on aromatic edge-to-face interactions was obtained using the

**Table 1** Interaction free energies ( $\text{kJ mol}^{-1}$ ) determined using zipper complexes in  $\text{CDCl}_3$  at  $296 \pm 2$  K. Errors are less than  $1 \text{ kJ mol}^{-1}$

Interaction	X	Y-Substituent			Fig.	Ref.
		NMe <sub>2</sub>	H	NO <sub>2</sub>		
	NMe <sub>2</sub>	-0.9	-1.1	-1.4	14	20, 21, 35
	H	-1.8	-1.4	-0.2		
	NO <sub>2</sub>	-4.6	-3.4	+1.2		
						
	NMe <sub>2</sub>	-1.6 <sup>a</sup>	-2.0 <sup>a</sup>	-2.4 <sup>a</sup>	14	31
	H	-1.8	-1.4	-0.2		
	NO <sub>2</sub>	-4.3	-3.1	-0.5		
						
	NMe <sub>2</sub>	-1.6 <sup>a</sup>			11b	36
	H	+0.9				
	NO <sub>2</sub>	+2.2 <sup>a</sup>				
						
		-3.6	-2.2	+2.1 <sup>b</sup>	14	37
		-2.8	-2.4	-0.9	11a	33
		-7.8	-2.5	+2.3	14	37–39
						
		-8.6	-4.6	+5.2	14	37
						
		-2.2	-2.2	-1.5	11a	57
						
		-2.4	-2.6	-1.8	11a	33
						
		-6.2	-4.7	-1.6	11a	33
			<-4.5		13	34
						
	F	+1.2 <sup>c</sup>	+2.8 <sup>c</sup>	+3.0 <sup>c</sup>		40
	Cl	+1.2 <sup>c</sup>	+1.5 <sup>c</sup>	+3.1 <sup>c</sup>	17a	40
	Br	+2.0 <sup>c</sup>	+1.2 <sup>c</sup>	+1.2 <sup>c</sup>		40
						
		+1.1	+0.8	-0.8	17c	30
						
	H	+1.5	+0.4	-0.8	17c	30
	NO <sub>2</sub>	-1.7	-2.3	+0.8	17d	
	F <sub>5</sub>	-3.2	-2.9	-0.2	17d	

<sup>a</sup> Unreliable due to differences in the conformation of these complexes as discussed in the original reference. <sup>b</sup> This value appears to deviate from the general trends and could be subject to an unknown source of error. <sup>c</sup> These values are likely to be perturbed by the steric restrictions of the zipper complex, and the low solubilities of the bisaniline derivatives used in <sup>1</sup>H NMR titrations.

semi-symmetrical zipper complexes made from compounds **17**, **26**, **27** and the appropriate mutant compounds for all combinations of X = NMe<sub>2</sub>, *t*-Bu, H, NO<sub>2</sub> and Y = NMe<sub>2</sub>, H and NO<sub>2</sub> (Fig. 14). The magnitudes of the edge-to-face interactions were found to correlate with Hammett substituent constants and electrostatic surface potentials demonstrating that electrostatic effects are primarily responsible for the differences in interaction energy (Fig. 12).<sup>31,35</sup> These findings substantiate the interaction trends observed in the fully symmetrical zipper complexes discussed above (Fig. 11a).

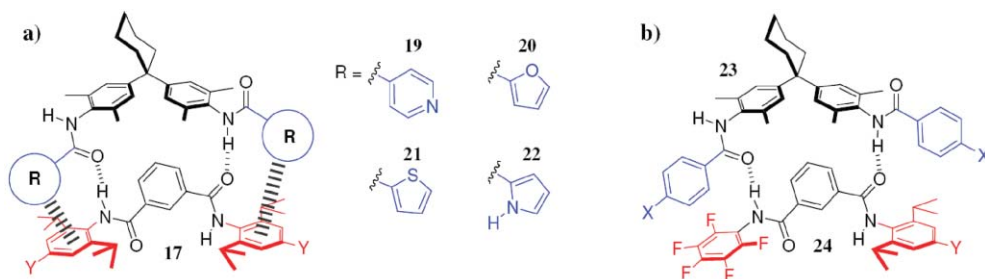
In order to test the role of electrostatics in aromatic interactions further, the effects of perfluorination of the face aromatic was investigated using compounds **23** and **24** where X = NMe<sub>2</sub>, *t*-Bu, H, F, I, CF<sub>3</sub> and NO<sub>2</sub> (Fig. 11b).<sup>36</sup> A symmetrical isophthaloyl derivative containing two terminal pentafluorophenyl groups (not shown) had very low solubility in CDCl<sub>3</sub> so was unsuitable for use in NMR titrations.<sup>29</sup> To overcome this difficulty, the unsymmetrical but soluble isophthaloyl derivative **24** and the corresponding mono-hexyl mutant were used with fully symmetrical bisaniline derivatives **23** to generate semi-symmetrical DMCs. The amide adjacent to the pentafluorophenyl group of **24** is a strong H-bond donor and weak H-bond acceptor, so a conformation in which this amide acts as a H-bond donor is preferred. This means that the geometry of the edge-to-face interaction is different from the non-fluorinated complexes in Fig. 14. The substituent-induced trend in the edge-to-perfluorinated face interaction was reversed compared to the non-fluorinated edge-to-face study, and this was attributed to the inversion of the electrostatic potential of the aromatic face caused by perfluorination.

The effect of substituents on the interaction between the edge of a pyridine ring and the face of Y-substituted phenyl rings was determined using unsymmetrical complexes of **28** and **17** (Fig. 14).<sup>37</sup> The interaction energies were similar to those determined using symmetrical complexes (Fig. 11a) when X = NMe<sub>2</sub> and H, but was substantially different when X = NO<sub>2</sub>. The reason for this difference is not clear, but the value measured in the symmetrical DMC is probably the more reliable result, since the system has fewer conformational possibilities. The value of +2.1 kJ mol<sup>-1</sup> appears to be unusually repulsive compared with the other edge-to-face interactions measured when Y = NO<sub>2</sub>. This suggests that a conformational problem may have affected the determination of this interaction energy.

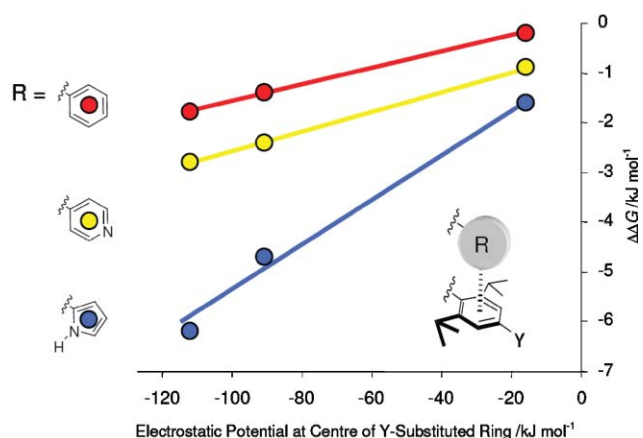
## Aromatic–cation interactions

Compound **28** can be easily *N*-methylated to yield **29**. Since compound **29** is a cation, this has allowed the effects of substituents on the cation– $\pi$  interaction to be measured using DMCs. The cation– $\pi$  interaction measured using **29**, mutant compounds and **17** where Y = NMe<sub>2</sub>, was measured as  $-7.8 \text{ kJ mol}^{-1}$  in CDCl<sub>3</sub> at 298 K, the most favourable interaction measured in the zipper complexes. Once again, the importance of the electrostatic properties of the aromatic groups in determining the strength of non-covalent interactions was demonstrated.<sup>38</sup> Cation– $\pi$  interactions were initially quantified using a hexafluorophosphate counter-ion. Although the choice of counter-ion affected the observed association



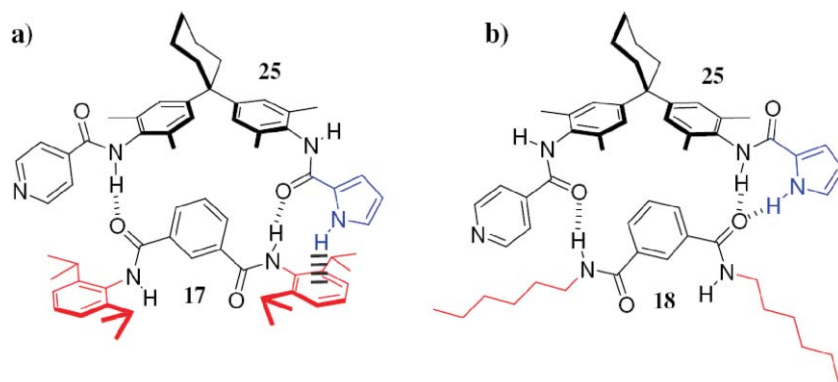


**Fig. 11** (a) Symmetrical bisaniline derivatives **19–22** used in  $^1\text{H}$  NMR titrations with **17** where  $\text{Y} = \text{NMe}_2, \text{H}$  and  $\text{NO}_2$ . (b) Compound **24** was used with **23** where  $\text{X} = \text{NMe}_2, t\text{-Bu}, \text{H}, \text{F}, \text{I}, \text{CF}_3$  and  $\text{NO}_2$ . Double-mutant cycles were constructed using single and double-mutant complexes; blue aromatic groups were mutated to  $t\text{-Bu}$  groups and red groups to  $n\text{-hexyl}$  chains as shown in Fig. 8.

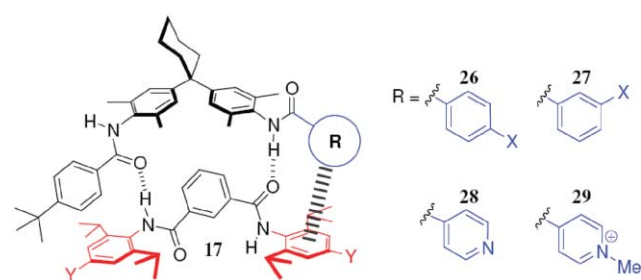


**Fig. 12** Plot of experimental edge-to-face aromatic interaction energies measured in zipper complexes ( $y$ -axis) against the B3LYP/6-31G\* calculated electrostatic surface potential at the ring centre of substituted isophthaloyl derivatives ( $x$ -axis from left to right  $\text{Y} = \text{NMe}_2, \text{H}$  and  $\text{NO}_2$ ). Errors are  $<1 \text{ kJ mol}^{-1}$ .

constants of the zipper complexes by almost three orders of magnitude, the cation- $\pi$  interaction (as dissected using DMCs) did not vary significantly with iodide, tetraphenyl borate and hexafluorophosphate counter-ions.<sup>39</sup> The effects of the anion on cation recognition events can simply be explained by the multiple equilibria present when the cation and anion compete for binding to each other and various sites on the host or guest.



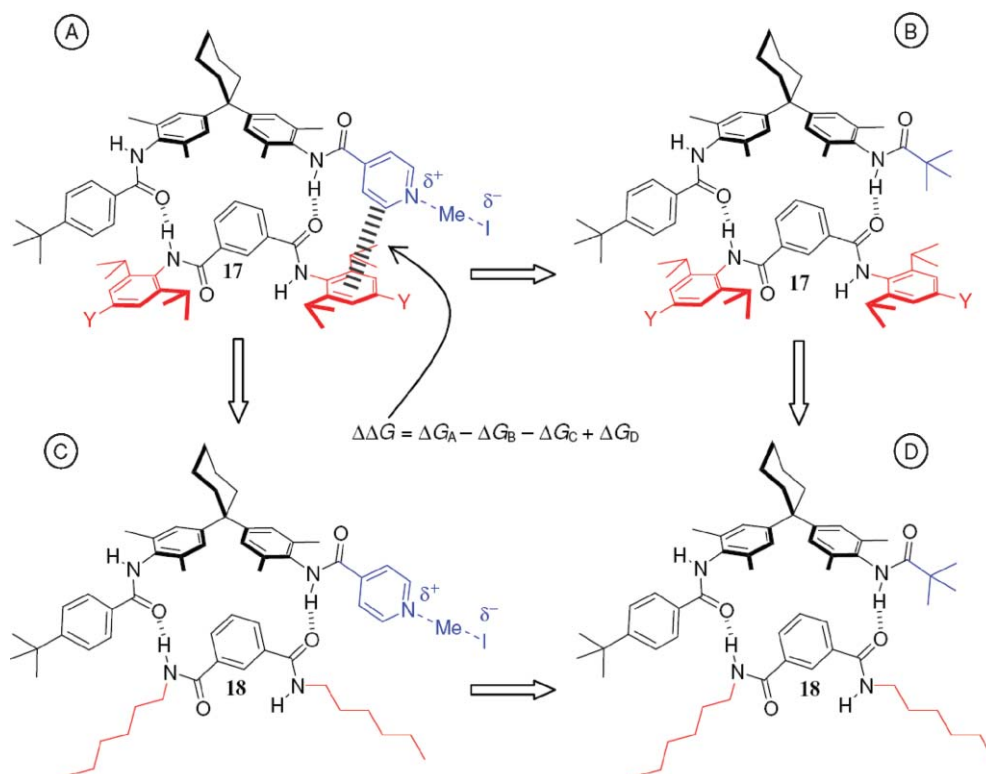
**Fig. 13** (a) Complex used for the measurement of the  $\text{NH}-\pi$  interaction. A double-mutant cycle was constructed using single and double-mutant complexes; the blue pyrrole group was mutated to a  $t\text{-Bu}$  group and the red aromatic rings to  $n\text{-hexyl}$  chains. (b) The preferred conformation of the **18-25** complex.



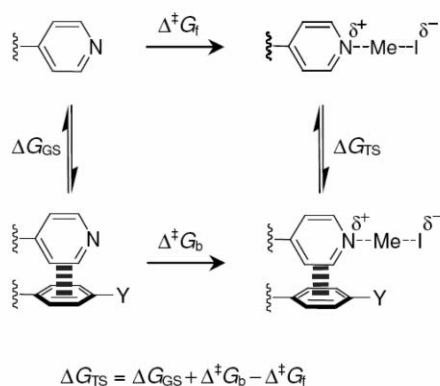
**Fig. 14** Semi-symmetrical complexes used for the measurement of the edge-to-face interaction between the substituted aromatic groups shown for all combinations of  $\text{X}$  and  $\text{Y} = \text{NMe}_2, \text{H}$  and  $\text{NO}_2$ . A double-mutant cycle was constructed using single and double-mutant complexes; the blue aromatic groups were mutated to a  $t\text{-Bu}$  group and the red aromatic rings to  $n\text{-hexyl}$  chains.

## Interactions in transition states

The  $N$ -methylation of compound **28** also provided the ideal opportunity to investigate functional group interactions in transition states.<sup>37</sup> Fig. 15 shows a DMC used for the quantification of the edge-to-face interaction in the *transition state* of the reaction between **28** and methyl iodide. This DMC requires association free energy differences that cannot be measured directly (complexes A and C). However, these values can be derived from the association constant of the ground state complex and the rates of the  $N$ -methylation reaction



**Fig. 15** Double-mutant cycle for determining the magnitude of the edge-to-face aromatic interaction in the transition state for the *N*-methylation of **28**.



**Fig. 16** Thermodynamic cycle used to evaluate the complexation free energy ( $\Delta G_{TS}$ ) of the transition state for the *N*-methylation of **28**.

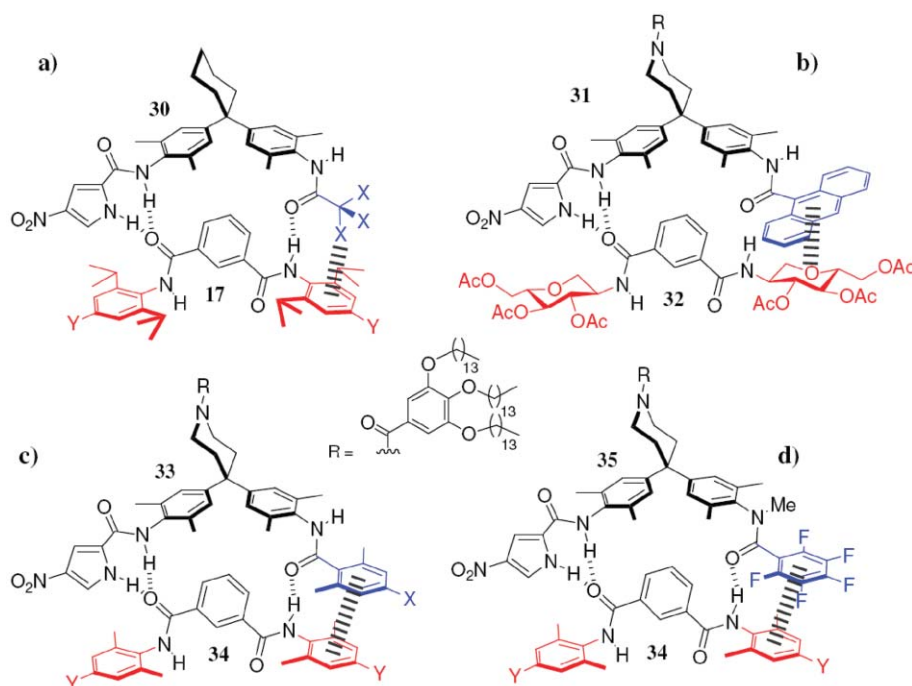
in the free and bound states as shown in Fig. 16. The interactions in the transition states were found to be larger than the interactions in the reactant (**28**) or the product (**29**), suggesting that aromatic rings can catalyse pyridine alkylation by stabilising the developing positive charge in the transition state.

### Aromatic–halogen interactions

The compounds shown in Fig. 17 all feature the nitropyrrole group which represented a significant advance in the design of the zipper complexes. The nitropyrrole group was introduced

based on the observation that the pyrrole-containing compound **25** bound the hexyl mutant isophthaloyl derivative **18** primarily in the conformation discussed above (Fig. 13b). It was realised that the pyrrole group could be used to ‘lock’ the conformation on one side of the complex.<sup>29</sup> Conformational control could be further improved by introduction of a nitro group. In addition, the association constants of the complexes were raised, allowing binding constants to be determined with greater accuracy. The introduction of the nitropyrrole unit did not come without disadvantages: the behaviour of the bisaniline compounds was complicated by additional conformational equilibria, increased levels of self-association and low solubility. Fortunately, the nitropyrrole conformers are minor, and self-association could be accounted for in analysis of the titration data. Both of these problems were shown to have little effect on the measured interaction free energies, since any associated systematic errors cancel in the DMC.<sup>29</sup>

The nitropyrrole functionality was used in complexes for investigation of the non-covalent interaction between halogens and the face of aromatic rings (Fig. 17a).<sup>40</sup> The interaction was found to be repulsive with all substituents ( $X = F, Cl, Br$  and  $Y = NMe_2, H$  and  $NO_2$ ). However, this supramolecular design was far from ideal, since the geometric constraints of the zipper framework and the variation in size of the halogen atoms mean that the measured interactions reflect steric as well as electrostatic effects. In addition, the low solubility of the bisaniline derivatives (**30**) in  $CDCl_3$  limited the coverage of the binding isotherm and therefore the accuracy of the measured association constants.



**Fig. 17** Nitropyrrole zipper complexes used for the measurement of (a) halogen- $\pi$  interactions, (b) carbohydrate- $\pi$  interactions, (c) aromatic stacking interactions, and (d) aromatic stacking interactions with electron-withdrawing aromatic groups on the bisaniline half of the complex. A double-mutant cycle was constructed using single and double-mutant complexes; the blue  $CX_3$  groups were mutated to *t*-Bu, the blue aromatic groups to methyl, and the red groups to *n*-hexyl chains.

### Aromatic-carbohydrate interactions

The solubility problem was solved by the attachment of a bulky solubilising group to the bisaniline derivatives in subsequent zipper designs. Using complexes similar to the example shown in Fig. 17b, carbohydrate- $\pi$  interactions were investigated.<sup>41</sup> The selection of appropriate amino-sugars allowed the interaction of each face of glucose and galactose derivatives with the anthracene group to be measured. The results of these studies are shown in Table 2. Complexation-induced changes in chemical shift indicated that these complexes were conformationally well-behaved. In particular, the small chemical shift of the amide proton adjacent to the anthracene group showed that the amide flipping problem

experienced in previous zipper complexes had been brought under control. The interaction between the carbohydrate derivatives and the anthracene group was found to be highly dependent upon which face of the carbohydrate group was brought into contact with the aromatic group. For both glucose and galactose derivatives, when the ring oxygen was pointed away from the aromatic face, the interaction was favourable. When the other face of the carbohydrate was oriented towards the face aromatic ring, the interaction became repulsive. These observations were attributed to multiple favourable CH- $\pi$  interactions between the carbohydrate and the aromatic group in one orientation, which are compensated by a stronger repulsive electrostatic interaction between the partially negatively-charged oxygen atoms and the aromatic surface in the other geometry.

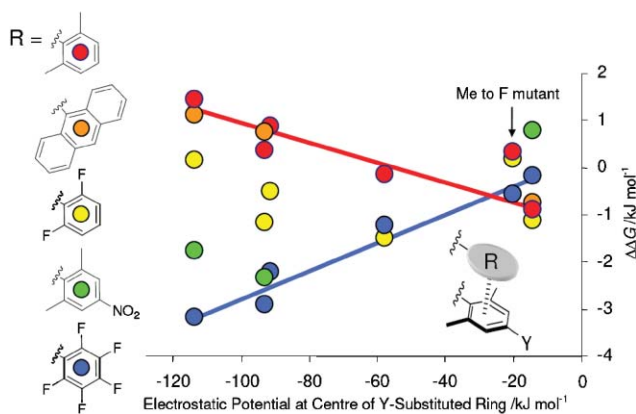
**Table 2** Free energies ( $\text{kJ mol}^{-1}$ ) for aromatic-carbohydrate interactions determined using zipper complexes in  $\text{CDCl}_3$  at 298 K. Errors are less than  $1 \text{ kJ mol}^{-1}$ .<sup>a</sup>

Interaction	X	$\Delta G/\text{kJ mol}^{-1}$	Interaction	$\Delta G/\text{kJ mol}^{-1}$
	OAc	+0.9		+3.8
	OMe	+1.3		
	OAc	-1.4		-1.0
	OMe	-1.1		

<sup>a</sup> All values from reference 41.

### Aromatic stacking interactions

The anthracene derivatised bisaniline derivative (**31**) used in the carbohydrate- $\pi$  study was also used for the investigation of aromatic stacking interactions.<sup>29</sup> The isopropyl groups of the isophthaloyl derivative (**17**) were replaced with less bulky methyl groups (**34**) to allow close intermolecular stacking in the zipper complex. The interaction was found to be repulsive with electron-rich aromatics ( $Y = \text{NMe}_2$  and H), but slightly attractive with electron-poor aromatics ( $Y = \text{NO}_2$ ). Modified stacking complexes (**33-34**) (Fig. 17c) gave almost identical results when  $X = \text{H}$  as the Y-substituents were varied. Although the complexes containing the anthracene group (**31**) and phenyl ring ( $X = \text{H}$ ) (**33**) were conformationally well-behaved with little evidence of amide flipping, the same was



**Fig. 18** Plot of experimental aromatic stacking interaction energies measured in zipper complexes ( $y$ -axis) against the B3LYP/6-31G\* calculated electrostatic surface potential at the ring centre of substituted isophthaloyl derivatives ( $x$ -axis from left to right,  $Y = \text{NMe}_2$ , H, OMe, Cl, H (with both methyl groups mutated to fluorine) and  $\text{NO}_2$ ). Errors are  $\sim 1 \text{ kJ mol}^{-1}$ .

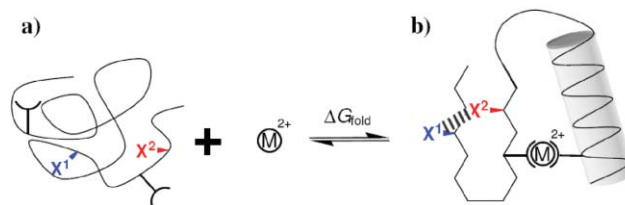
not true when  $X = \text{NO}_2$  or when this terminal ring was replaced with a pentafluorophenyl group.<sup>22</sup> Electron-withdrawing aromatic groups make the adjacent amide a strong H-bond donor and a weak H-bond acceptor causing the amide flipping problem to re-emerge, in addition to reducing the solubility of these compounds in  $\text{CDCl}_3$ . This problem was overcome by  $N$ -methylation of the offending amide, allowing a detailed study of substituent effects on aromatic stacking interactions.<sup>42</sup>

The major trends in the stacking interaction energies could be explained using a simple electrostatic model. Electron-rich aromatics repel one another, and the interaction approaches zero as the electrostatic potential of either ring surface nears zero. Replacement of a phenyl group or anthracene group with pentafluorophenyl inverted the substituent-induced interaction trend (Fig. 18). This is due to the positive surface of the pentafluorophenyl group compared to the negative surfaces of anthracene and benzene. Additional electrostatic interactions between methyl protons and electron-rich aromatic surfaces were identified by mutating methyl groups to fluorine atoms.

DMCs can also be used to dissect individual non-covalent interaction terms from theoretical energies determined by computational calculations. This approach has been used successfully in combination with the XED force-field, and it seems that the removal of systematic errors by the DMC leads to rather reliable functional group interaction energies that compare remarkably well with experiment.<sup>36,43,44</sup> For the wide range of interactions with aromatic rings that have been characterised in Sheffield, both experiment and molecular mechanics calculations point to the dominant role of electrostatics in determining the trends in interaction free energies.

## Folding molecules

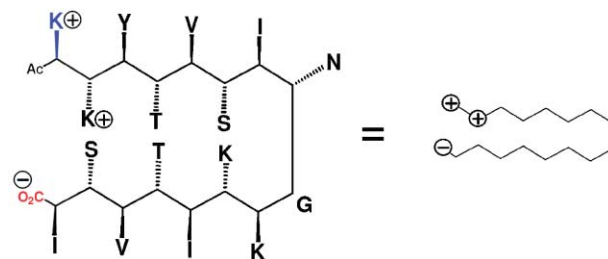
DMC methodology can be applied to the study of non-covalent interactions in folding molecules that present two-state conformational behaviour (*i.e.* distinct folded and unfolded states).<sup>45</sup> Simple peptides which exhibit suitable



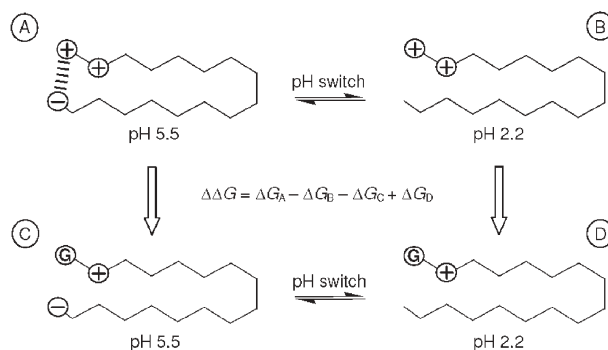
**Fig. 19** Schematic representation of the folding equilibrium of a zinc finger peptide studied by Blasie and Berg. In the folded state (b) amino acid side-chains  $X^1$  and  $X^2$  are brought into close proximity.

folding characteristics have been studied in combination with the DMC methodology. Blasie and Berg studied electrostatic interactions across a  $\beta$ -sheet in a 26-residue zinc finger peptide.<sup>46</sup> In the absence of metal, the peptide is largely or completely unfolded. Upon binding of zinc(II) or cobalt(II), the peptide adopts a well-defined tertiary structure and amino acid side chains  $X^1$  and  $X^2$  are brought into close proximity (Fig. 19). With the assumption that amino acid mutations not involving the metal binding residues do not affect the direct interactions between the peptide and the metal ion, changes in metal binding represent a measure of the relative folding energies of each peptide sequence. Metal binding was measured in 100 mM HEPES buffer using a competitive two-peptide metal binding assay and co-titrations were monitored using UV spectroscopy. Electrostatic interactions between solvent-exposed salt bridges (residues  $X^1$  and  $X^2$ ) were isolated using the DMC approach (Fig. 1). It was found that stabilising interaction energies were modest,  $< 2 \text{ kJ mol}^{-1}$  at NaCl concentrations of 0–100 mM. The results suggest that the interactions are effectively buffered by a combination of solvent competition and conformational entropic penalties.

The two-state folding approximation is valid for many minimal  $\beta$ -peptide hairpin sequences. Searle took advantage of this situation to elucidate the electrostatic and hydrophobic contributions to the stability of the folded state in a 16-residue  $\beta$ -hairpin (Fig. 20).<sup>47</sup> This peptide shows little preference for the folded state or unfolded state at pH 5.5 at 298 K, therefore changes in the folding ratio can be used as a sensitive measure of the effects of non-covalent interactions and environmental effects. Folding free energies were calculated from the folded/unfolded ratio, which was determined from differences in NMR chemical shift relative to peptide random coils (unfolded state) and the fully folded state (in 50% aqueous methanol at



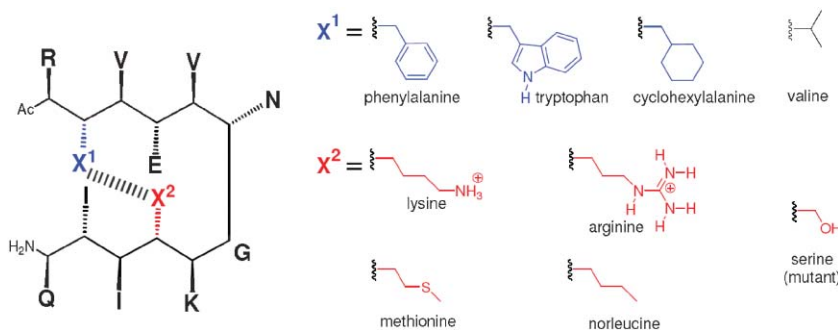
**Fig. 20** Schematic representation of the  $\beta$ -hairpin peptides used by Searle for the investigation of non-covalent interactions. Side chains are indicated by the one letter amino acid code. The blue lysine residue was replaced by glycine in the mutant compound.



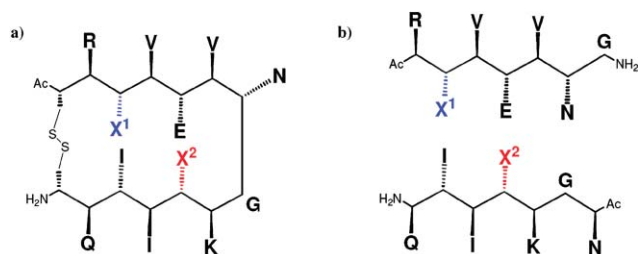
**Fig. 21** Double-mutant cycle constructed by Searle and co-workers for the quantification of the electrostatic interaction between a protonated lysine side-chain and a carboxylate group in the  $\beta$ -hairpin peptide shown in Fig. 20. In the mutant  $\beta$ -hairpin, lysine is replaced with glycine (G). The second mutation is brought about by a change in pH.

278 K). The DMC shown in Fig. 21 was constructed using a single mutant  $\beta$ -hairpin, in which the lysine residue was replaced with glycine (G). The second mutation is brought about by a change in pH. The C-terminal carboxylate group of isoleucine has a  $pK_a$  of 3.4, so at pH 2.2 it has no net charge, but at pH 5.5 it is deprotonated. Using the DMC in Fig. 21, the favourable electrostatic interaction between the terminal carboxylate group and the protonated lysine group on the opposing side of the  $\beta$ -hairpin was measured as 1.0–1.2  $\text{kJ mol}^{-1}$ . A series of assumptions allowed the contribution of the hydrophobic effect to the stability of the folded hairpin to be estimated at 0.3–0.8  $\text{kJ mol}^{-1}$ .

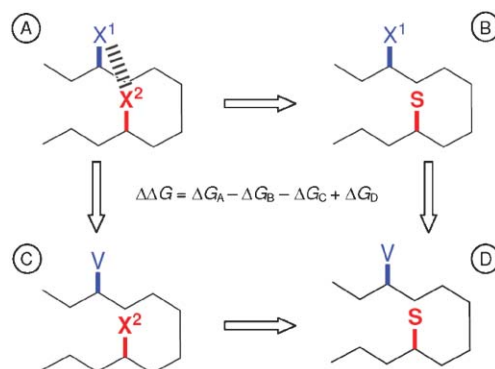
Tatko and Waters have also used  $\beta$ -hairpins to study non-covalent interactions in a biologically relevant environment. The 12-residue peptide sequence used in a number of studies in combination with the DMC methodology is shown in Fig. 22. Serine and valine were selected as the mutant residues. As in the study of Searle, the fraction folded was determined using  $^1\text{H}$  NMR spectroscopy. However, Tatko and Waters used the control compounds in Fig. 23 to obtain reference chemical shifts corresponding to the folded and unfolded states. Using the DMC shown in Fig. 24, various diagonal  $X^1$  and  $X^2$  side chain combinations were investigated, and the interactions between them quantified from the free energies determined from folded fractions (Table 3).<sup>48–50</sup> Tatko and Waters have also used DMCs to measure cross-strand side



**Fig. 22** Schematic representation of the  $\beta$ -hairpin peptides used by Tatko and Waters for the measurement of the diagonal interaction between side chains  $X^1$  and  $X^2$ . Unvarying side chains are indicated by one letter amino acid codes.



**Fig. 23** NMR reference peptides corresponding to (a) the folded state and (b) the unfolded state.



**Fig. 24** Double-mutant cycle used by Tatko and Waters for the quantification of diagonal non-covalent interactions between the  $X^1$  and  $X^2$  side-chains in a  $\beta$ -hairpin.

chain interactions (*cf.* diagonal interactions) using  $\beta$ -peptides. Folding free energies were determined using the approach described above, but with a different peptide (Fig. 25). Using these peptides, the interaction between two cross-strand phenylalanine residues was determined to be  $-2.3 \text{ kJ mol}^{-1}$ .<sup>51</sup>

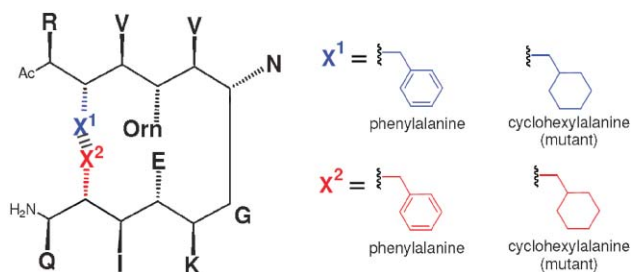
Interpretation of the results obtained in peptide systems is difficult because of the inherent flexibility of these molecules and the sensitivity of non-covalent interactions to changes in geometry. The measured free energy differences reflect the interactions between the side chains as well as the energetic contributions from desolvation. These energy contributions are intrinsically coupled and are hard to separate, because increased polarity leads to a larger desolvation cost.<sup>9</sup> Nevertheless, the studies of folding of peptide systems presented here are among the first systematic investigations to have isolated the energetic contributions of pairwise

**Table 3** Interaction free energies ( $\text{kJ mol}^{-1}$ ) determined in  $\beta$ -hairpin peptides in  $\text{D}_2\text{O-H}_2\text{O}$  at 298 K by Tatko and Waters. Errors are less than  $0.5 \text{ kJ mol}^{-1}$

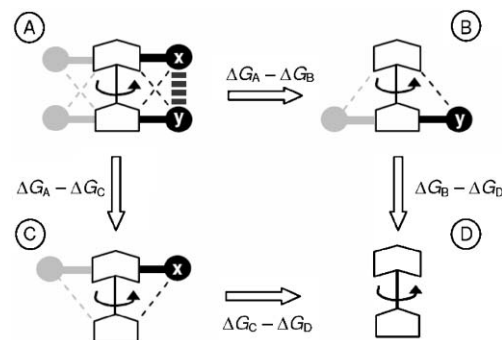
$X^2 X^1$	Lysine	Arginine	Methionine	Norleucine
Phenylalanine	-0.8	-1.2	-1.3	-0.4
Tryptophan	-1.5	-1.9	-1.3	-0.8
Cyclohexylalanine	-0.4	—	-2.1	-1.3

interactions by taking secondary effects into account. Such fundamental studies are of undoubted importance in the tackling the huge challenge presented by the complexities of protein folding.

Returning to the opposite end of the folding molecule spectrum, minimal synthetic folding systems, such as the 'torsion balance' molecules developed by Oki and Wilcox have been extensively used for the study of non-covalent interactions.<sup>52–55</sup> Both of these systems have been exploited by other investigators.<sup>56–59</sup> Distinct foldamer signals in NMR spectra indicate that folding is a two-state event on the NMR timescale. Integration of the conformer NMR signals at equilibrium gives a direct measure of the folding free energy. A DMC may not be necessary to take secondary interactions into account in folding molecules which possess a high degree of symmetry. As shown in Fig. 26, if a single mutation completely removes the rotating group, or if the remaining linking group is identical in the folded and unfolded states, then the same secondary interactions are present in the folded and unfolded state. In fact, the molecule ceases to be a foldamer for mutations B, C and D. In practice, such ideal symmetry is rarely achieved, because the functional groups of interest are often connected to the framework of the torsion balance molecule *via* an intermediate linkage that provides a source of secondary interactions. Even so, in some systems, a



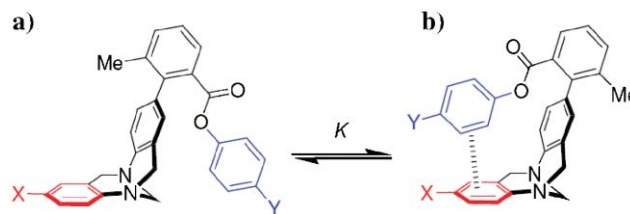
**Fig. 25** Schematic representation of the  $\beta$ -hairpin peptides used by Tatko and Waters for the measurement of the cross-strand aromatic-aromatic interaction between two phenylalanine side chains. Unvarying side chains are indicated by one letter amino acid codes, except Orn = ornithine.



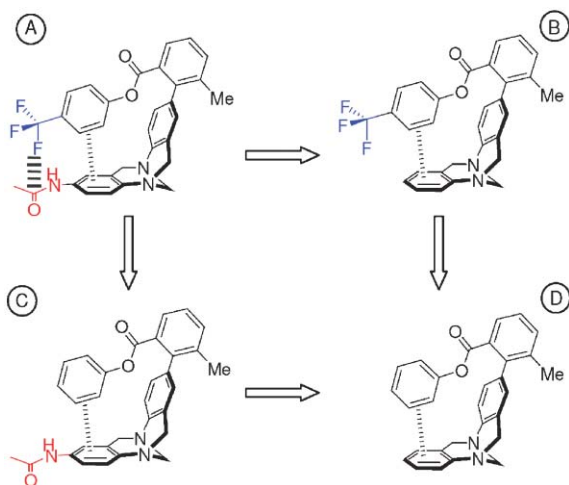
**Fig. 26** General schematic representation of a double-mutant cycle for measurement of the  $x$ - $y$  interaction in a folding molecule. The bold broken line represents the non-covalent interaction of interest and the fine broken lines the secondary effects that are cancelled in the cycle. Grey shadows represent the unfolded states.

single mutation may prove to be the equivalent of performing a complete DMC.

To demonstrate the principle, we take the molecular torsion balance of Wilcox as an example (Fig. 27). The simplicity of the system means that potential secondary interactions which could affect the folding equilibrium are easily identified. Taking the edge-to-face interaction between the Y- and X-substituted rings as the interaction of interest, secondary interactions can be identified as involving the edge aromatic and ester group with the other aromatic ring in the system. However, these contacts also occur in the unfolded state.



**Fig. 27** The 'molecular torsion balance' developed by Wilcox for the quantification of  $\text{CH-}\pi$  interactions: (a) the unfolded state; (b) the folded state which contains the  $\text{CH-}\pi$  interaction.



**Fig. 28** DMC used by Diederich for the quantification of the interaction between fluorine and an amide group in folded state A.

Theoretically these secondary effects should cancel in the folding equilibrium, but experimentally determined folding free energies of mutant compounds where the edge aromatic is replaced by a methyl group reveal that the folding behaviour is not as simple as expected.<sup>55</sup> A second mutation would involve the removal of the face aromatic. Such a mutation would leave a compound which was almost perfectly symmetrical along the rotating bond axis, and it can be assumed that the folding free energy is zero or very close to zero. Thus, the measurement of the edge-to-face interaction can be achieved (whilst accounting for secondary effects) by a single mutation of the edge aromatic; the approach taken by Wilcox in the most recently published molecular torsion balance studies.<sup>55</sup>

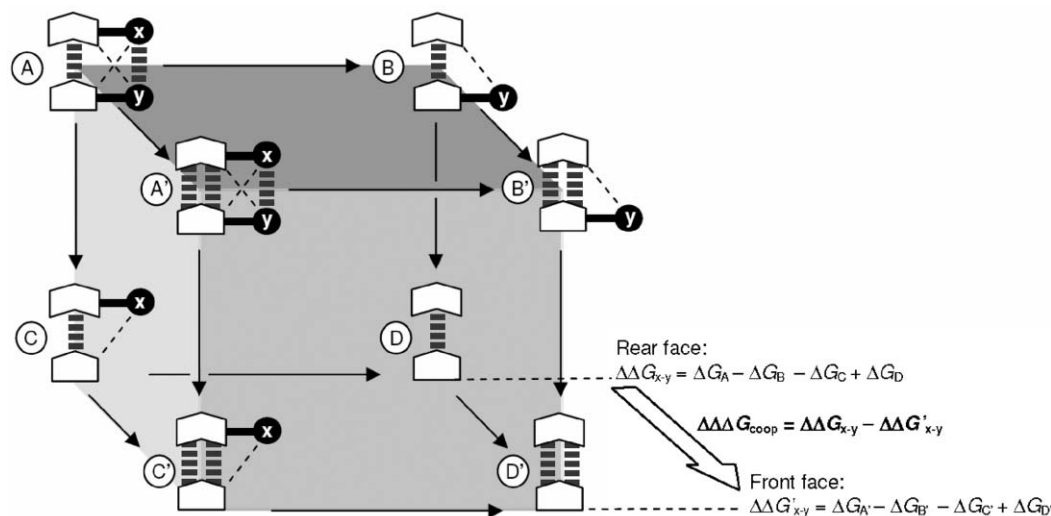
Diederich made use of the Wilcox torsion balance framework for the measurement of a weak attractive interaction between organic fluorine and an amide group (Fig. 28).<sup>59</sup> The folding equilibrium in compound A is controlled by the

interaction of interest as well as edge-to-face interactions, solvation and other secondary effects.<sup>60</sup> In order to factor out the edge-to-face interaction and other secondary interactions, Diederich constructed the DMC shown in Fig. 28. The fluorine to amide interaction was measured as  $-0.8$  to  $1.5$   $\text{kJ mol}^{-1}$  in three different non-polar solvents. A linear free energy relationship showed that the edge-to-face interaction at the heart of the folding molecules was a function of the electronic properties of the face aromatic as substituents were varied in  $\text{C}_6\text{D}_6$ , confirming that the requirement of additivity is satisfied.

### Triple-mutant boxes

It has been shown how DMCs can be used in a variety of situations to isolate and measure individual functional group interactions. However, the DMC energy may still be affected by cooperativity. The combination of two different DMCs that measure the same interaction results in a construct known as a triple-mutant box (TMB). Using a triple-mutant box, it is possible to assess the effect of cooperativity between intermolecular interactions. Like the DMC, the TMB was pioneered in the protein engineering field and has been used to quantify cooperativity in a number of proteins.<sup>2,61–65</sup>

Fig. 29 shows a schematic representation of a TMB as applied to a supramolecular system. Complexes A–D at the rear of the TMB contain a single anchoring interaction and form a typical DMC that can be used to measure the  $x$ – $y$  interaction as described above. Complexes A'–D' at the front of the box form another DMC which quantifies exactly the same  $x$ – $y$  interaction in an unchanged environment, but each complex possesses an additional anchoring interaction and is therefore more stable than the corresponding complexes A–D. Thus, the free energy difference between the front and rear faces (*i.e.*  $\Delta\Delta G_{x-y} - \Delta\Delta G'_{x-y}$ ) is a measure of the cooperative effect of the additional anchoring interaction on the  $x$ – $y$  interaction.



**Fig. 29** Schematic representation of a supramolecular triple-mutant box used to quantify the cooperative effects of an additional anchoring interaction on the  $x$ – $y$  interaction. The bold broken lines represent the major non-covalent interactions in the supramolecular complex and the fine broken lines are secondary effects.

We have used DMCs and TMBs to assess cooperativity in zipper complexes of different stabilities.<sup>66</sup> Three DMCs were constructed using zipper oligomers of differing lengths: complexes were held together by two (Fig. 8), three or four H-bonds (Fig. 7). The sum of the two terminal edge-to-face interactions (X and Y = H) was measured as  $-2.6$ ,  $-3.2$  and  $-2.6$   $\text{kJ mol}^{-1}$  using DMCs for complexes that vary in stability by  $14$   $\text{kJ mol}^{-1}$ . TMBs determined the cooperative effects to be  $-0.5$ ,  $-0.3$  and  $+0.2$   $\text{kJ mol}^{-1}$ , *i.e.* within the experimental error. However, for such weak functional group interactions, the magnitudes of any cooperative effects might be expected to be too small to be accurately determined by this approach: changes of at least 30% in the free energy of interaction would be required. We addressed the limitations of this study by measuring cooperative effects in zipper complexes involving substantially larger interactions.<sup>12</sup> To obtain a measure of cooperativity, it is not necessary to dissect individual interaction terms, *i.e.* two complete DMCs are not required. The difference in the measured energies of the same group of interactions in complexes of different overall stability is sufficient to provide a measurement of cooperativity (*e.g.* a cycle involving the A–A'–C–C' face of the triple-mutant box in Fig. 29). Using this approach, the cooperative effect was measured as  $0.2 \pm 0.4$   $\text{kJ mol}^{-1}$  for composite functional group interaction free energies of 8–13  $\text{kJ mol}^{-1}$ . These results support the assumption that the individual interaction terms are additive in the DMC zipper complexes, since the free energies of individual functional group interactions are independent of the overall stability of the complex. Additionally, these findings demonstrate that the enthalpic chelate effect, which has been discussed as a possible cause of non-additivity in biological interactions, does not have an impact on the behaviour of these synthetic systems.<sup>67–71</sup>

## Conclusion

The double-mutant cycle is a robust thermodynamic tool that can be used to isolate individual weak non-covalent interactions from the noisy background of multiple secondary interactions. The approach has been widely used in the study of protein interactions, but it has seen limited application in synthetic chemical systems. The behaviour of the most diminutive chemical systems are often perturbed by secondary effects, and many systems are compatible with the approach, provided that appropriate single and double mutant controls are synthesised. Key studies that have employed the DMC methodology have been discussed from supramolecular complexes, to folding peptides and torsion balance molecules. It has been shown how the triple-mutant box (or part of one) can be used to clarify the role of cooperative effects.

## Acknowledgements

We thank F. Hoffmann-La Roche Ltd. (S.L.C.) for funding.

## References

- 1 P. J. Carter, G. Winter, A. J. Wilkinson and A. R. Fersht, *Cell*, 1984, **38**, 835–840.
- 2 A. Horovitz and A. R. Fersht, *J. Mol. Biol.*, 1990, **214**, 613–617.

- 3 L. Serrano, A. Horovitz, B. Avron, M. Bycroft and A. R. Fersht, *Biochemistry*, 1990, **29**, 9343–9352.
- 4 G. A. Faiman and A. Horovitz, *Protein Eng.*, 1996, **9**, 315–316.
- 5 M. D. Distefano, A. Zhong and A. G. Cochran, *J. Mol. Biol.*, 2002, **322**, 179–188.
- 6 C. K. Vaughan, P. Harryson, A. M. Buckle and A. R. Fersht, *Acta Crystallogr., Sect. D: Biol. Crystallogr.*, 2002, **D58**, 591–600.
- 7 E. Di Cera, *Chem. Rev.*, 1998, **98**, 1563–1591.
- 8 G. Schreiber, *Biomol. Sens.*, 2002, 19–32.
- 9 C. A. Hunter, *Angew. Chem., Int. Ed.*, 2004, **43**, 5310–5324.
- 10 H. J. Schneider, T. Schiestel and P. Zimmermann, *J. Am. Chem. Soc.*, 1992, **114**, 7698–7703.
- 11 G. Ercolani, *J. Am. Chem. Soc.*, 2003, **125**, 16097–16103.
- 12 C. A. Hunter and S. Tomas, *Chem. Biol.*, 2003, **10**, 1023–1032.
- 13 A. Camara-Campos, C. A. Hunter and S. Tomas, *Proc. Natl. Acad. Sci. U. S. A.*, 2006, **103**, 3034–3038.
- 14 Y. Aoyama, M. Asakawa, A. Yamagishi, H. Toi and H. Ogoshi, *J. Am. Chem. Soc.*, 1990, **112**, 3145–3151.
- 15 Y. Aoyama, M. Asakawa, Y. Matsui and H. Ogoshi, *J. Am. Chem. Soc.*, 1991, **113**, 6233–6240.
- 16 D. Gust, T. A. Moore, P. A. Liddell, G. A. Nemeth, L. R. Makings, A. L. Moore, D. Barrett, P. J. Pessiki, R. V. Bensasson, M. Rougee, C. Chachaty, F. C. De Schryver, M. Van der Auweraer, A. R. Holzwarth and J. S. Connolly, *J. Am. Chem. Soc.*, 1987, **109**, 846–856.
- 17 Y. Kato, M. M. Conn and J. Rebek, Jr., *J. Am. Chem. Soc.*, 1994, **116**, 3279–3284.
- 18 A. P. Bisson, F. J. Carver, C. A. Hunter and J. P. Waltho, *J. Am. Chem. Soc.*, 1994, **116**, 10292–10293.
- 19 A. P. Bisson, F. J. Carver, D. S. Eggleston, R. C. Haltiwanger, C. A. Hunter, D. L. Livingstone, J. F. McCabe, C. Rotger and A. E. Rowan, *J. Am. Chem. Soc.*, 2000, **122**, 8856–8868.
- 20 H. Adams, F. J. Carver, C. A. Hunter, J. C. Morales and E. M. Seward, *Angew. Chem., Int. Ed. Engl.*, 1996, **35**, 1542–1544.
- 21 F. J. Carver, C. A. Hunter, P. S. Jones, D. J. Livingstone, J. F. McCabe, E. M. Seward, P. Tiger and S. E. Spey, *Chem.–Eur. J.*, 2001, **7**, 4854–4862.
- 22 S. L. Cockcroft, C. A. Hunter, K. R. Lawson, J. Perkins and C. J. Urch, *J. Am. Chem. Soc.*, 2005, **127**, 8594–8595.
- 23 C. A. Hunter, M. J. Packer and C. Zonta, *Prog. Nucl. Magn. Reson. Spectrosc.*, 2005, **47**, 27–39.
- 24 C. A. Hunter and M. J. Packer, *Chem.–Eur. J.*, 1999, **5**, 1891–1897.
- 25 A. Spitaleri, C. A. Hunter, J. F. McCabe, M. J. Packer and S. L. Cockcroft, *CrystEngComm*, 2004, **6**, 489–493.
- 26 M. Gardner, A. J. Guerin, C. A. Hunter, U. Michelsen and C. Rotger, *New J. Chem.*, 1999, **23**, 309–316.
- 27 C. A. Hunter, C. M. R. Low, M. J. Packer, S. E. Spey, J. G. Vinter, M. O. Vysotsky and C. Zonta, *Angew. Chem., Int. Ed.*, 2001, **40**, 2678–2682.
- 28 H. Adams, P. L. Bernad, Jr., G. A. Hembury, C. A. Hunter, J. F. McCabe, D. S. Eggleston, R. C. Haltiwanger, D. J. Livingstone, K. D. M. Harris and B. M. Kariuki, *Chem. Commun.*, 2001, 1500–1501.
- 29 H. Adams, C. A. Hunter, K. R. Lawson, J. Perkins, S. E. Spey, C. J. Urch and J. M. Sanderson, *Chem.–Eur. J.*, 2001, **7**, 4863–4877.
- 30 J. Perkins, PhD Thesis, University of Sheffield, 1999.
- 31 F. J. Carver, C. A. Hunter, D. J. Livingstone, J. F. McCabe and E. M. Seward, *Chem.–Eur. J.*, 2002, **8**, 2847–2859.
- 32 A. García Martínez, J. Osio Barcina and A. De Fresno Cerezo, *Chem.–Eur. J.*, 2001, **7**, 1171–1175.
- 33 J. F. McCabe, PhD Thesis, University of Sheffield, 1997.
- 34 H. Adams, K. D. M. Harris, G. A. Hembury, C. A. Hunter, D. Livingstone and J. F. McCabe, *Chem. Commun.*, 1996, 2531–2532.
- 35 F. J. Carver, C. A. Hunter and E. M. Seward, *Chem. Commun.*, 1998, 775–776.
- 36 H. Adams, J.-L. J. Blanco, G. Chessari, C. A. Hunter, C. M. R. Low, J. M. Sanderson and J. G. Vinter, *Chem.–Eur. J.*, 2001, **7**, 3494–3503.
- 37 C. A. Hunter, C. M. R. Low, J. G. Vinter and C. Zonta, *J. Am. Chem. Soc.*, 2003, **125**, 9936–9937.
- 38 C. A. Hunter, C. M. R. Low, C. Rotger, J. G. Vinter and C. Zonta, *Proc. Natl. Acad. Sci. U. S. A.*, 2002, **99**, 4873–4876.



- 
- 39 C. A. Hunter, C. M. R. Low, C. Rotger, J. G. Vinter and C. Zonta, *Chem. Commun.*, 2003, 834–835.
- 40 H. Adams, S. L. Cockcroft, C. Guardigli, C. A. Hunter, K. R. Lawson, J. Perkins, S. E. Spey, C. J. Urch and R. Ford, *ChemBioChem*, 2004, **5**, 657–665.
- 41 A. Lea, PhD Thesis, University of Sheffield, 2002.
- 42 S. L. Cockcroft, PhD Thesis, University of Sheffield, 2006.
- 43 J. G. Vinter, *J. Comput. Aided Mol. Des.*, 1994, **8**, 653–668.
- 44 G. Chessari, C. A. Hunter, C. M. R. Low, M. J. Packer, J. G. Vinter and C. Zonta, *Chem.–Eur. J.*, 2002, **8**, 2860–2867.
- 45 M. S. Searle and B. Ciani, *Curr. Opin. Struct. Biol.*, 2004, **14**, 458–464.
- 46 C. A. Blasie and J. M. Berg, *Biochemistry*, 1997, **36**, 6218–6222.
- 47 M. S. Searle, S. R. Griffiths-Jones and H. Skinner-Smith, *J. Am. Chem. Soc.*, 1999, **121**, 11615–11620.
- 48 C. D. Tatko and M. L. Waters, *Protein Sci.*, 2003, **12**, 2443–2452.
- 49 C. D. Tatko and M. L. Waters, *J. Am. Chem. Soc.*, 2004, **126**, 2028–2034.
- 50 C. D. Tatko and M. L. Waters, *Protein Sci.*, 2004, **13**, 2515–2522.
- 51 C. D. Tatko and M. L. Waters, *J. Am. Chem. Soc.*, 2002, **124**, 9372–9373.
- 52 M. Oki, M. Nishino, K. Kaieda, T. Nakashima and S. Toyota, *Bull. Chem. Soc. Jpn.*, 2001, **74**, 357–361.
- 53 M. Oki, *Acc. Chem. Res.*, 1990, **23**, 351–356.
- 54 S. Paliwal, S. Geib and C. S. Wilcox, *J. Am. Chem. Soc.*, 1994, **116**, 4497–4498.
- 55 E.-i. Kim, S. Paliwal and C. S. Wilcox, *J. Am. Chem. Soc.*, 1998, **120**, 11192–11193.
- 56 B. W. Gung, X. Xue and H. J. Reich, *J. Org. Chem.*, 2005, **70**, 7232–7237.
- 57 B. W. Gung, X. Xue and H. J. Reich, *J. Org. Chem.*, 2005, **70**, 3641–3644.
- 58 T. Ren, Y. Jin, K. S. Kim and D. H. Kim, *J. Biomol. Struct. Dyn.*, 1997, **15**, 401–405.
- 59 F. Hof, D. M. Scofield, W. B. Schweizer and F. Diederich, *Angew. Chem., Int. Ed.*, 2004, **43**, 5056–5059.
- 60 S. L. Cockcroft and C. A. Hunter, *Chem. Commun.*, 2006, 3806–3808.
- 61 A. Horovitz and A. R. Fersht, *J. Mol. Biol.*, 1992, **224**, 733–740.
- 62 J. Steyaert and L. Wyns, *J. Mol. Biol.*, 1993, **229**, 770–781.
- 63 G. Schreiber, C. Frisch and A. R. Fersht, *J. Mol. Biol.*, 1997, **270**, 111–122.
- 64 J. Steyaert, A. F. Haikal and L. Wyns, *Proteins: Struct., Funct., Genet.*, 1994, **18**, 318–323.
- 65 J. S. Redzic and B. E. Bowler, *Biochemistry*, 2005, **44**, 2900–2908.
- 66 C. A. Hunter, P. S. Jones, P. Tiger and S. Tomas, *Chem.–Eur. J.*, 2002, **8**, 5435–5446.
- 67 S. Jusuf, P. J. Loll and P. H. Axelsen, *J. Am. Chem. Soc.*, 2003, **125**, 3988–3994.
- 68 S. Jusuf, P. J. Loll and P. H. Axelsen, *J. Am. Chem. Soc.*, 2002, **124**, 3490–3491.
- 69 S. Jusuf and P. H. Axelsen, *Biochemistry*, 2004, **43**, 15446–15452.
- 70 H. Shiozawa, B. C. S. Chia, N. L. Davies, R. Zerella and D. H. Williams, *J. Am. Chem. Soc.*, 2002, **124**, 3914–3919.
- 71 J. Rao, J. Lahiri, R. M. Weis and G. M. Whitesides, *J. Am. Chem. Soc.*, 2000, **122**, 2698–2710.